Porphyromonas gingivalis induces entero-hepatic metabolic derangements with alteration of gut microbiota in a type 2 diabetes mouse model

Yoichiro Kashiwagi
Osaka University

Syunsuke Aburaya
Kyushu University

Naoyuki Sugiyama
Kyoto University

Yuki Narukawa
Osaka University

Yuta Sakamoto
Kyoto University

Masatomo Takahashi
Kyushu University

Hayato Uemura
Kyoto University

Rentaro Yamashita
Kyoto University

Syotaro Tominaga
Osaka University

Satoko Hayashi
Osaka University

Takenori Nozaki
Osaka University

Satoru Yamada
Osaka University

Yoshihiro Izumi
Kyushu University

Atsunori Kashiwagi
Kusatsu general hospital

Takeshi Bamba
Kyushu University

Yasushi Ishihama
Kyoto University

Shinya Murakami (✉ ipshinya@dent.osaka-u.ac.jp)
Osaka University

Abstract

Periodontal infection is thought to generate systemic inflammation, thus aggravating diabetes. Furthermore, orally administered periodontal pathogens may directly alter the gut microbiota. To elucidate this, using an obese *db/db* diabetes mice, orally treated with *Porphyromonas gingivalis* (*Pg*), we screened for *Pg*-specific peptides in intestinal fecal specimens and examined whether *Pg* localization affected the intestinal microbiota profile altering gut metabolite levels. Finally, we screened whether deterioration of fasting hyperglycemia was related to changes in intrahepatic glucose metabolism, using proteome and metabolome analyses. As results; (1) Oral *Pg* treatment aggravated both fasting and postprandial hyperglycemia ($P < 0.05$) with a significant ($P < 0.01$) increase in dental alveolar bone resorption. (2) *Pg*-specific peptides were identified in fecal specimens after oral *Pg* treatment and intestinal *Pg* profoundly altered gut microbiome profiles at the phylum, family, and genus levels. *Prevotella* showed the largest increase in abundance. Furthermore, *Pg*-treatment significantly altered intestinal metabolite levels. (3) Fasting hyperglycemia was associated with increases in gluconeogenesis-related enzyme and metabolite levels without changes in proinflammatory cytokine expressions and insulin resistance. This work reveals that oral *Pg* administration induced gut microbiota changes, leading to entero-hepatic metabolic derangements, thereby aggravating hyperglycemia in an obese type 2 diabetes mouse model.

Introduction

Human oral biofilm-forming bacteria cause chronic inflammatory periodontal infection due to a bacterial symbiosis disorder caused by inadequate oral hygiene [1,2]. *Porphyromonas gingivalis* (*Pg*) is the most common periodontal pathogen causing periodontitis in periodontal pockets [3,4]. Inflammatory cytokines are reportedly chronically overproduced in accelerated periodontitis, which may exacerbate systemic metabolic diseases [5–7].

The clinical association of periodontal diseases with poor glycemic control of diabetes has been actively investigated [5]. It is generally accepted that diabetes is a major risk factor for periodontal disease, with a 3-fold-higher prevalence of periodontitis in diabetic patients than in non-diabetic subjects, and poor glycemic control may trigger and worsen periodontitis in diabetes [8–10]. However, advanced stages of periodontitis may further impair glycemic control in diabetic patients [11]. Although the mechanisms connecting these conditions remain elusive, it has been speculated that local infection by oral pathogens, and release of inflammatory cytokines into blood vessels, may explain the systemic effects of periodontal disease [5–7, 12].

However, recent studies have proposed that the dissemination of periodontal pathogens into the intestinal tract may induce systemic inflammation, metabolic changes, and fatty liver disease in non-diabetic mice models [13,14]. Clarifying this requires identification of orally administered periodontal bacteria in fecal specimens. However, bacterial cells and their genomic DNA have not been previously identified in fecal specimens, likely due to their rapid digestion by intestinal enzymes [13,14].

Here, we studied the presence of *Pg* in fecal specimens at the peptide level, using proteomic analysis of *Pg*-specific peptide fragments after oral administration of *Pg* in obese type 2 diabetes mice. It is known that oral bacteria mixed with saliva and food can survive in the acidic stomach environment, and subsequently be transmitted to the intestinal tract with food [15].

We found that oral administration of *Pg* in diabetic mice aggravated both fasting and postprandial hyperglycemia, and increased alveolar bone reabsorption. Excessive hepatic gluconeogenesis contributes to hyperglycemia in poorly controlled diabetes [16,17]. Therefore, using genomic, proteomic, or metabolomic analyses, we investigated whether *Pg*-administration increased mRNA and protein expression of hepatic gluconeogenesis-related enzymes, intrahepatic glucose, and lipid metabolites in diabetic mice. Furthermore, previous studies have used metagenome analysis to study changes in of gut microbiota of *Pg*-treated diabetic mice [13,18]; in this study, we applied metaproteome analysis to elucidate this.

Results

Increased fasting and postprandial hyperglycemia following *Pg*-treatment

Blood glucose under *ad libitum* feeding in *Pg*-administered mice was significantly ($P < 0.05$) higher than in control mice, 3 and 4 weeks after oral treatment. However, neither body weight nor food intake differed significantly between the two groups (Table 1). Fasting serum glucose levels were significantly higher ($P < 0.05$) in *Pg*-treated than control mice, but their fasting hyperinsulinemia and serum triglyceride levels were similar (Table 2). Although both fasting and postprandial glucose 2 h after glucose loading were higher in *Pg*-treated mice, the area under the glucose excursion curve after the oral glucose tolerance test was not significantly different from that in the control

(Supplementary Table S1). The intraperitoneal insulin tolerance test showed a similar reduction in glucose levels between the *Pg*- and carboxymethyl cellulose (CMC)- treated mice (Supplementary Table S1).

Increased alveolar bone resorption following *Pg* treatment

To assess periodontitis severity, bone loss on the buccal side of the maxillary alveolar bone was measured at five points using μCT image analysis. *Pg*-treated mice exhibited statistically significant ($P < 0.01$) alveolar bone resorption compared to control mice (Fig. 1a,1b).

Detection of *Pg*-specific peptides and changes in the microbiome profile of fecal specimens

Six distinct peptides derived from *Pg* were identified by proteome analysis of the mouse feces in *Pg*- and CMC-treated mice (Table 3). The specific detection of the *Pg*-derived peptides in *Pg*-treated mice was quantitatively assessed by PRM analysis using a synthetic peptide as an internal standard. *Pg*-specific peptides in fecal specimens were detected in *Pg*-treated, but not CMC (control)-treated, mice (Fig. 2a, b).

The phylum-level microbial composition of the fecal microbiome was analyzed using LC-MS/MS-based shotgun metaproteome analyses. Approximately 350,000 MS/MS spectra per sample were obtained, and were submitted for screening against the UniProt database of all putative proteins in the mouse gut metagenome [19], the murine UniProt proteome database, and against the proteomes of the food items and *Pg*. The number of peptides identified in the proteome analysis did not differ substantially between the *Pg*- and CMC-treated groups (Table 4). In total, 16,974 unique peptides were identified. Among them, 5,576 taxon-specific peptides were matched to 14 phyla of microbes, 2,451 peptides to 58 families, and 1,626 peptides to 111 genera (Supplementary Table S2).

Bacteroidetes and Firmicutes dominated the gut microbiota in both *Pg*-treated and control mice (Fig. 2c). After the 30 d treatment period, the Bacteroidetes population (as a proportion of all bacteria present) was larger, whereas the Firmicutes population was smaller in the *Pg*-treated mice than in the control group (Firmicutes/Bacteroides: 68%/30% in the *Pg*-treated group and 50%/49% in the control group). At the family level, *Prevotellaceae* comprised a higher proportion in the *Pg*-treated group (27%) than in the control (10%) (Fig. 2d). *Prevotella*, the most abundant genus in the fecal samples, was present at a higher proportion in the *Pg*-treated group (37%) than in the control (14%) (Fig. 2e).

Changes in intestinal metabolites following *Pg* treatment

Metabolome analysis of mixed samples of small intestinal tissues and fecal materials showed marked differences in intestinal metabolites between *Pg*- and CMC-treated mice. The volcano plots compare the metabolite levels in the fecal specimens of *Pg*- and CMC-treated mice. Following *Pg*-treatment, twelve hydrophilic metabolites were significantly elevated, whereas 35 were significantly reduced (Fig. 3). Many end metabolites, such as lactate, phosphoric acid, 3-hydroxybutyric acid, 3-hydroxyisobutyric acid, a valine metabolite, and *O*-phosphoethanolamine, a metabolite of sphingosine-1-phosphate, were significantly higher in the *Pg*-treated mice than in the control mice (Table 5). In contrast, the levels of many amino acids and polyamines in were significantly lower in the *Pg*-treated mice than in the control mice (Table 5).

Changes in Rate-limiting enzyme expression and glucose metabolites levels in the liver of *Pg*-treatment diabetic mice

Enhanced fasting hyperglycemia is regulated by hepatic gluconeogenesis in poorly controlled diabetes. To determine whether hepatic gene and protein expression levels related to gluconeogenesis were enhanced in *Pg*-treated mice, the expression of phosphoenolpyruvate carboxykinase (*Pck1*) and Glucose 6 phosphatase (*G6pc*) was determined. *Pck1* mRNA expression was significantly higher in *Pg*-treated mice than control mice ($P < 0.05$), but *G6pc* mRNA expression did not differ significantly between the treatment and control groups (Fig. 4a). Gene expression of Forkhead box protein O1 (*Foxo1*), a transcription factor in hepatocytes that promotes gluconeogenesis to activate *Pck1* and *G6pc* expression, was also significantly higher in *Pg*-treated mice than in the control. *Cytochrome P450 A1* (*Cyp 7a1*), a rate-limiting enzyme involved in bile acid biosynthesis, was significantly higher ($P < 0.01$) in the livers of *Pg*-treated mice than in the control. We further compared the hepatic protein expression of PCK1 and FOXO1 between the *Pg*-treated and control mice. Western blot analysis revealed higher PCK1 and FOXO1 protein expression in *Pg*-treated mice ($P < 0.05$) than in the control (Fig. 4b). Immunohistochemical

analyses revealed upregulated PCK1 and FOXO1 expression in the livers of *Pg*-treated mice relative to levels in the control (Fig. 4c, d). In contrast, gene expression of fatty acid synthase (*Fasn*) was significantly downregulated (*P* < 0.05), and acetyl-CoA carboxylase A (*Acaca*) gene expression was lower, in the livers of *Pg*-treated mice, relative to levels in the control. Hepatic lipogenesis-related genes, *Srebf1* and *Srebf2*, did not differ significantly between *Pg*-treated and control mice (Fig. 4a). mRNA expression of Il-6, Tnf-a, Ccl2, and Cxcl10 were not significantly different between the treatment and control (Fig. 4e).

To clarify enhanced fasting hyperglycemia in diabetic mice following oral *Pg*-administration, the enzyme protein, glucose and lipid metabolite levels in the liver were quantified via proteomic and metabolomic analyses. There was significant differential expression between the treatment and control groups, such as a 1.2-fold increase, or more than a 0.83-fold reduction, in the *Pg*-treated mice relative to levels in the control (*P* < 0.05). The volcano plots of hepatic glucose metabolites (Fig. 5a) reveal that levels of 396 proteins, 42 hydrophilic metabolites, and 62 lipids were elevated following *Pg*-treatment, relative to the control. Notably, levels of 444 proteins, 6 hydrophilic metabolites, and 12 lipids were lower following *Pg*-treatment than in the control (Fig. 5a). Comparative metabolomic analysis revealed that *Pg*-administration significantly reduced glycogen storage in the liver relative to that in the control, and increased levels of metabolites related to gluconeogenesis and the *tricarboxylic acid cycle* (TCA) cycle, such as PEP, PGA, FUM, and MAL, in the liver (*P* < 0.05) (Fig. 5b). Comparative proteome analysis revealed that levels of the enzymes involved in glycogen synthesis and degradation, and in G6P metabolism via the glycolytic pathway (namely, Gys2, AGL, Pgm2, and Gpi1) were significantly lower in the treatment than in the control (Fig. 5c). Levels of the glycolysis/gluconeogenesis-related proteins PCK1, Tpi1, and Aldoa, were significantly (*P* < 0.05) higher, whereas those of Diat, Pdhb, and Ldha were significantly lower (*P* < 0.05) in the treatment than in the control (Fig. 5d). We showed a summary of the changes in hepatic glucose metabolite levels and the rate-limiting enzyme expressions of glucose metabolism were coincident with enhanced gluconeogenesis in the Pg-treated diabetic mice as compared with the CMC-treated mice (Fig. 6). Furthermore, no significant differences in fatty acid, glycerides, cholesterol, cholesterol ester, phospholipid, and sphingolipid contents were observed between the treatment and control groups (Supplementary Fig. S1).

Discussion

This study revealed the presence of specific *Pg*-derived peptides in fecal specimens from *db/db* diabetic mice after 30 days after oral *Pg*-administration, via proteomic analysis. *Pg*-treatment significantly altered the gut microbiota composition. Various intestinal metabolites were altered in the mixed intestinal tissue and feces samples from *Pg*-treated mice. These changes were associated with aggravated reabsorption of maxillary alveolar bone and of both fasting and postprandial hyperglycemia. Furthermore, the proteome and metabolome analyses revealed that these metabolic changes were associated with differential expression of glucose-metabolism rate-limiting enzymes and intrahepatic glucose metabolites, but not with changes in insulin resistance and hepatic proinflammatory cytokine expression, following Pg-treatment.

Our findings confirm the hypothesis [15] that oral bacteria mixed with saliva and food are able to pass through the stomach and reach the intestinal tract. A previous metagenome analysis [15] reported relative proportions of *Firmicutes* and *Bacteroides* after oral *Pg*-treatment of 55.4% and 38.7%, respectively, in *Pg*-treated mice, and 72.8% and 17.0%, in control mice, respectively.. In the present study, we confirmed these findings via proteomics. Furthermore, the microbiome changes were larger after the 10th *Pg*-treatment period than after a single treatment of *Pg* (Fig. 2c).

Prevotellaceae and *Prevotella* populations were higher in *Pg*-treated mice than in the control mice (Fig. 2d, 2e). Notably, oral administration of periodontal pathogenic bacterium *Aggregatibacter actinomycetemcomitans* has also been shown to alter gut microbiota composition in a non-diabetic mouse model [14], with enhanced hepatic fat deposition, which differs from the present results. Gut dysbiosis induced by periodontal pathogens is associated with biological effects such as increased intestinal permeability to low molecular weight metabolites produced by invading bacteria. Those metabolites are delivered to the liver, where they may impair glucose tolerance and insulin resistance while also activating cytokine expression [13,14]. Conversely, several studies have indicated that changes in specific beneficial metabolites improve whole-body glucose metabolism and intestinal barrier function [20,21], or help to control obesity [22]. Here, we observed remarkable changes in various intestinal metabolites following *Pg*-treatment, with no changes in systemic proinflammatory cytokine levels. Interestingly, it has been reported that there are close links[23,24] between *Prevotella*, which we found to be more abundant in *Pg*-treated mice, and oral and gastrointestinal tract diseases. Therefore, in future work we intend to study how *Prevotella* species in the intestinal microbiota respond to oral administration of periodontal bacteria.

The liver is crucial for maintaining normal glucose homeostasis, by altering glycogen synthesis and degradation, glycolysis, and gluconeogenesis, depending on the fasting and postprandial states. In type 2 diabetes with poor glycemic control, hepatic glucose output is regulated by gluconeogenesis [16,17], via changes in insulin, and insulin-counter-regulatory hormones, and catecholamine action, and

insulin-counter-regulatory hormones and the supply of gluconeogenic substrates [17,25,26]. We found that oral Pg-administration upregulated hepatic gluconeogenesis-related enzymes at mRNA and protein expression levels in diabetic mice. It has already been reported that oral administration of periodontal pathogens impairs both glucose tolerance and insulin sensitivity in non-diabetic mice and in streptozotocin-induced diabetic mice [13,14,18], which are related to the increased hepatic gene expression of proinflammatory cytokines [13,18]. However, in the present study, Pg-treatment did not alter the gene expression of proinflammatory cytokines, relative to levels in the control mice(Fig. 4e). Furthermore, Pg-administration reportedly induces fatty liver and raises hepatic triglyceride levels in a non-diabetic mouse model [13]. In contrast, our results indicate that orally administered Pg did not modify triglyceride levels in either the blood or liver, relative to levels in CMC-treated diabetic mice; similarly, it did not increase the gene expressions of fatty acid biosynthesis-related enzymes Fasn, Acaca, Srebf1, and Srebf2 in the present study.

This study is focused on the upregulation of hepatic gluconeogenesis after oral Pg-administration in diabetic mice. FOXO1 is the most direct transcriptional regulator of gluconeogenesis [27]. We observed consistently increased FOXO1 and PCK1 gene and protein expressions in Pg-treated diabetic mice, but not significant in G6pc gene expression in the present study. Although activation of FOXO1 and PCK1 gene and protein expression may be related to enhanced gluconeogenesis activity, it still remains unclear whether dysregulation of the FOXO1 transcription factor mainly contributes to the increased rates of gluconeogenesis rates observed in type 2 diabetes [26,28]. In addition, extrahepatic supply of gluconeogenic precursor substrates such as glycerol, lactate, and alanine from fat and muscle cells may be necessary in vivo. In the present study, we used the same liver samples for metabolome and proteome analyses. Consistent with previous reports on patients with type 2 diabetes [29], we found that Pg-treatment reduced glycogen storage levels. Glycerol released from fat cells is incorporated in the liver and is converted to DHAP and then GAP via Tpi1 (Fig. 6). These metabolites are essential for gluconeogenesis via conversion of GAP to FBP and DHAP to F1P via aldolase (Aldoa). Both Aldoa and Tpi1 were upregulated in Pg-treated mice relative to the control in the present study. Alanine released from skeletal muscle cells is converted to pyruvate via alanine aminotransferase (ALT), and lactate is converted to pyruvate via lactate dehydrogenase (Ldha) in the liver. Pyruvate is then converted to oxaloacetate via pyruvate carboxylase. Oxaloacetate is then converted to PEP via PCK1. Our western blotting, proteome analyses and real time PCR revealed increased PCK1 protein and mRNA expression following Pg-treatment. In contrast, lactate dehydrogenase and pyruvate dehydrogenase B expression was downregulated, indicating limited pyruvate flow to the TCA cycle, and increased pyruvate flow to the gluconeogenesis pathway. Furthermore, both fumaric acid (FUM) and malic acid (MAL) contents were higher following Pg-treatment. In Pg-treated mice, it is possible that these metabolites promote hepatic gluconeogenesis by supplying oxaloacetate. Thus, our findings of altered hepatic content of glucose metabolites and the rate-limiting glucose-metabolism enzymes following Pg-treatment are consistent with enhanced gluconeogenesis in Pg-treated db/db mice. In contrast, consistent with previous reports[29], we found that Pg-treatment further reduced glycogen storage in the liver of db/db mice indicating that glucose incorporation into glycogen was further decreased by the PG-treatment in the diabetic mice. However, it should be noted that such changes in hepatic glucose metabolites could also be induced by hepatic enzyme activities due to increased plasma insulin-counter regulatory hormone levels [30,31], which were not extensively measured in the present study.

In conclusion, we first identified Pg-specific peptides in fecal specimens from obese type 2 diabetes model mice given oral Pg for 30 days. Proteome analysis revealed that the presence of Pg in the intestine significantly altered the gut microbiome profile at phylum, family, and genus levels. Pg-treatment significantly altered the local contents of intestinal end metabolites, many amino acids, and polyamines. Finally, Pg-treatment aggravated both fasting and postprandial glucose levels, and increased gluconeogenesis-related metabolite contents and enzyme expressions. However, we did not find further increased proinflammatory cytokine expressions in the liver and insulin resistance in the Pg-treated db/db mice, which were typical characteristics in obese type 2 diabetes model mice.

Methods

Animals

Forty-one male C57BLKS/Jlar+Lepr/db+Lepr/db (db/db) mice aged 6 weeks were purchased from Japan SLC, Inc. (Shizuoka, Japan). They were maintained under controlled temperature (23±2 °C) and light-dark cycle with free access to food and water, and fed a regular chow diet (5.1% fat, 55.3% carbohydrate, 23.1% protein; MF Oriental Yeast Co., Ltd., Tokyo, Japan). After acclimatization for a week, the mice were randomly assigned to Pg-treated (n = 20) and CMC-treated (n = 21) groups. The bacterial load administered in the mouse periodontitis model was based on Baker et al. [32]. Pg and CMC were administered orally through a plastic tube, with 10^9 CFU Pg mixed with 4% CMC () (for the Pg-treatment), or only CMC (for the control), every 3 d for 30 d. Livers were excised after anesthetization using mixed anesthesia (Domitor, 0.75 mg/kg body weight; Midazolam, 4 mg/kg; and Butorphanol Tartrate, 5 mg/kg), and were flash-frozen in liquid nitrogen.

The oral glucose tolerance test was performed following overnight (10 h) fasting. Fasting glucose levels were measured, and mice were orally administered with 2 g glucose/kg body weight. The intraperitoneal insulin tolerance test was conducted by intraperitoneal insulin injections (5 units/kg body weight). Blood glucose levels were measured at 0, 30, 60, and 120 min after insulin administration.

To determine insulin levels, blood samples were collected from the inferior vena cava of anesthetized mice. Serum insulin levels were determined using the insulin ELISA kit (FujiFilm Wako Shibayagi Corporation, Gunma, Japan), following the manufacturer's instructions.

All animal experiments were performed according to the protocols approved by the institutional animal care and use committees of Osaka University Graduate School of Dentistry (permit number: 27-022-0) and were in accordance with the Guide for the Care and Use of Laboratory Animals, published by the National Academies Press. All mice were manipulated in accordance with Animal Research Reporting In Vivo Experiments (ARRIVE) guidelines.

Bacterial culture

The *Pg* strain (ATCC33277) was obtained from the American Type Culture Collection (ATCC, Manassas, VA) and grown at 37 °C for 24 h in an anaerobic box chamber (Mitsubishi Gas Chemical Company, Inc. Tokyo, Japan) with AnaeroPack-Anaero anaerobic gas generator (Mitsubishi Gas Chemical Company, Inc.) in Gifu anaerobic medium supplemented with 5 mg/mL yeast extract, 5 µg/mL hemin, and 0.2 µg/mL vitamin K1.

Quantification of alveolar bone resorption

Morphometric analysis of buccal alveolar bone resorption was performed using an R_mCT2 3D micro X-ray computed tomography system designed for use with scanned images of laboratory animals (Rigaku, Tokyo, Japan). An examiner blinded to the experimental groups measured the linear distances of the cementoenamel junction (CEJ) from the alveolar bone crest (ABC) using the 3D image analysis software TRI/3D-BON (RATOC System Engineering Co., Ltd., Tokyo, Japan). Five linear points were measured on each molar root surface (three on the distal root, two on the mesial root).

Real-time PCR

Total RNA from the mouse liver was extracted using an RNeasy lipid tissue mini kit (Qiagen, Venlo, Netherlands) according to the manufacturer's instructions. cDNA was synthesized from 100 ng total RNA using a high-capacity cDNA archive kit (Applied Biosystems, Foster City, CA). PCR was performed using the ABI 7300 real-time PCR system with the Power SYBR Green PCR master mix (both from Applied Biosystems) according to the manufacturer's protocol. To control for variation in the amount of DNA available for PCR, target gene expression in each sample was standardized based on expression of an endogenous control. The sequences of the primers used are provided in Supplementary Table S3.

Protein analysis

Total proteins were extracted from the frozen livers using the T-PER tissue protein extraction reagent (Thermo Fisher Scientific Inc., Waltham, MA), and used for western blotting. Immunoblotting was performed using the following primary antibodies: PCK1 (ab28455, Abcam, Toronto, Canada), G6PC (ab83690; Abcam), FOXO1 (2880, Cell Signaling Technology, Danvers, MA), and b-actin (A5216, Sigma-Aldrich Co., St. Louis, MO).

Histology

Liver tissues, excised from mice after the 30 days period of oral administration of *Pg*- and CMC-treatment, were fixed using 4% paraformaldehyde for 48 h and embedded in paraffin. The tissue sections were then deparaffinized, rehydrated, and washed with PBS. The tissue sections were cut at 4 µm and stained with hematoxylin and eosin (H&E). For immunohistochemistry, samples were embedded in

paraffin, sectioned, and stained with rabbit anti-PCK1 (ab2845, 0.4 µg/mL; Abcam) and rabbit anti-FOXO1 antibodies (2880, 0.2 µg/mL; Cell Signaling Technology). Positive staining was visualized using a Simple Stain DAB Solution.

Metabolome analysis

Metabolites were extracted from the frozen small intestines or frozen livers using Bligh and Dyer's method [33]. Metabolome analysis of the small intestines was performed at the Chemicals Evaluation and Research Institute (CERI, Saitama, Japan) via gas chromatography triple quadrupole mass spectrometry (GC/MS/MS) and ion-paring liquid chromatography triple quadrupole mass spectrometry (ion-pairing LC/MS/MS) [34]. Hydrophilic metabolites of the liver were analyzed using ion chromatography coupled with a high-resolution tandem mass spectrometer (IC/MS/MS) for anionic polar metabolites such as organic acids and nucleotides [35], and liquid chromatography with a pentafluorophenyl propyl column coupled with a high-resolution tandem mass spectrometer (PFPP-LC/MS/MS) for cationic polar metabolites such as amino acids [35]. The free fatty acid (FA) and cholesteryl ester (ChE) lipid content of the livers was quantified using supercritical fluid chromatography with a C18 column coupled with triple quadrupole mass spectrometry (C18-SFC/MS/MS) [36]. The levels of other lipids—phosphatidylcholine (PC), phosphatidylethanolamine (PE), phosphatidylserine (PS), phosphatidylglycerol (PG), phosphatidylinositol (PI), phosphatidic acid (PA), lysophosphatidylcholine (LPC), lysophosphatidylethanolamine (LPE), monoacylglycerol (MG), diacylglycerol (DG), triacylglycerol (TG),   sphingomyelin (SM), cholesterol, ceramide (Cer), and hexosylceramide (HexCer)—were quantified using SFC with a diethylamine (DEA) column coupled with triple quadrupole mass spectrometry (DEA-SFC/MS/MS) [37]. Details regarding sample preparation and the analytical conditions for hydrophilic and hydrophobic metabolite analysis are provided as Supplementary Methods.

Determination of liver glycogen content

The glycogen content of liver tissue was determined using an aqueous size-exclusion chromatographic method previously reported [38].

Proteome analysis of liver enzymes and gut microbiota in fecal specimens

Liver and fecal samples of the 12-week-old male *db/db* mice After the 30 days treatment were collected and cut into small pieces with dissection scissors. For fecal samples, 450 µL methanol was added to 10 mg feces, and then 90 µL of the suspension was diluted with 450 µL methanol. Distilled water (250 µL) and 500 µL chloroform were added to the diluted suspension, followed by vortexing. After centrifugation at 4,600 ´ g for 5 min, both the organic and aqueous phases were removed, and pellets in the interphase were dried under vacuum. Proteins were extracted from the dried extract of the feces and the disrupted livers using the phase-transfer surfactant method [39] with a slight modification. The extracted protein was subjected to reductive alkylation, followed by successive digestion with Lys-C endopeptidase and trypsin, as previously described [40].

The mouse liver digests were isotopically labelled with TMT 10-plex [41] (Thermo Fisher Scientific) according to the manufacturer's protocol. For parallel reaction monitoring (PRM) analysis, the digests of fecal samples and of the synthetic peptide were isotopically labelled via reductive dimethylation [42]. The digested peptides were analyzed using nano-LC/MS/MS, using an Orbitrap Fusion Lumos mass spectrometer (Thermo Fisher Scientific) in data-dependent acquisition (DDA) mode, or using a Q Exactive mass spectrometer (Thermo Fisher Scientific) in PRM mode, coupled to Ultimate3000 RSLCnano system (CTC Analytics) and HTC-PAL autosampler (CTC). Details regarding sample preparation, the analytical conditions for nano-LC/MS/MS, and data processing, are described in the Supplementary Methods.

Statistical analysis

All data are presented as mean ± SEM. Differences in body weight, food intake, and blood glucose level between the *Pg* and CMC (control) groups were analyzed using one-way ANOVA with Tukey's post hoc test. All other comparisons between the two groups were analyzed using an unpaired *t*-test. Differences were considered statistically significant at $P < 0.05$.

References

1. Amar, S. & Han, X. The impact of periodontal infection on systemic diseases. *Med Sci Monit.***9**, RA291–299 (2003).

2. Tronstad, L. Recent development in endodontic research. *Scand J Dent Res.***100**, 52–59 https://doi.org/10.1111/j.1600-0722.1992.tb01809.x (1992).

3. Darveau, R. P., Hajishengallis, G. & Curtis, M. A. Porphyromonas gingivalis as a potential community activist for disease. *J Dent Res.***91**, 816–820 https://doi.org/10.1177/0022034512453589 (2012).

4. Hajishengallis, G., Darveau, R. P. & Curtis, M. A. The keystone-pathogen hypothesis. *Nat Rev Microbiol.***10**, 717–725 https://doi.org/10.1038/nrmicro2873 (2012).

5. Graziani, F., Gennai, S., Solini, A. & Petrini, M. A systematic review and meta-analysis of epidemiologic observational evidence on the effect of periodontitis on diabetes An update of the EFP-AAP review. *J Clin Periodontol.***45**, 167–187 https://doi.org/10.1111/jcpe.12837 (2018).

6. Saito, T., Shimazaki, Y. & Sakamoto, M. Obesity and periodontitis. *N Engl J Med.***339**, 482–483 https://doi.org/10.1056/NEJM199808133390717 (1998).

7. Yoneda, M. *et al.* Involvement of a periodontal pathogen, Porphyromonas gingivalis on the pathogenesis of non-alcoholic fatty liver disease. *BMC Gastroenterol.***12**, 16 https://doi.org/10.1186/1471-230X-12-16 (2012).

8. Cutler, C. W., Machen, R. L., Jotwani, R. & Iacopino, A. M. Heightened gingival inflammation and attachment loss in type 2 diabetics with hyperlipidemia. *J Periodontol.***70**, 1313–1321 https://doi.org/10.1902/jop.1999.70.11.1313 (1999).

9. Bridges, R. B., Anderson, J. W., Saxe, S. R., Gregory, K. & Bridges, S. R. Periodontal status of diabetic and non-diabetic men: effects of smoking, glycemic control, and socioeconomic factors. *J Periodontol.***67**, 1185–1192 https://doi.org/10.1902/jop.1996.67.11.1185 (1996).

10. Campus, G., Salem, A., Uzzau, S., Baldoni, E. & Tonolo, G. Diabetes and periodontal disease: a case-control study. *J Periodontol.***76**, 418–425 https://doi.org/10.1902/jop.2005.76.3.418 (2005).

11. Taylor, G. W. Periodontal treatment and its effects on glycemic control: a review of the evidence. *Oral Surg Oral Med Oral Pathol Oral Radiol Endod.***87**, 311–316 https://doi.org/10.1016/s1079-2104(99)70214-3 (1999).

12. Preshaw, P. M. *et al.* Periodontitis and diabetes: a two-way relationship. *Diabetologia.***55**, 21–31 https://doi.org/10.1007/s00125-011-2342-y (2012).

13. Arimatsu, K. *et al.* Oral pathobiont induces systemic inflammation and metabolic changes associated with alteration of gut microbiota. *Sci Rep.***4**, 4828 https://doi.org/10.1038/srep04828 (2014).

14. Komazaki, R. *et al.* Periodontal pathogenic bacteria, Aggregatibacter actinomycetemcomitans affect non-alcoholic fatty liver disease by altering gut microbiota and glucose metabolism. *Sci Rep.***7**, 13950 https://doi.org/10.1038/s41598-017-14260-9 (2017).

15. Schmidt, T. S. *et al.* Extensive transmission of microbes along the gastrointestinal tract. *Elife.***8**, https://doi.org/10.7554/eLife.42693 (2019).

16. DeFronzo, R. A. Pathogenesis of type 2 diabetes mellitus. *Med Clin North Am***88**, 787–835, ix, doi:10.1016/j.mcna.2004.04.013 (2004).

17. Zhang, X., Yang, S., Chen, J. & Su, Z. Unraveling the Regulation of Hepatic Gluconeogenesis. *Front Endocrinol (Lausanne).***9**, 802 https://doi.org/10.3389/fendo.2018.00802 (2018).

18. Ohtsu, A. *et al.* Influence of Porphyromonas gingivalis in gut microbiota of streptozotocin-induced diabetic mice. *Oral Dis.***25**, 868–880 https://doi.org/10.1111/odi.13044 (2019).

19. Xiao, L. *et al.* A catalog of the mouse gut metagenome. *Nat Biotechnol.***33**, 1103–1108 https://doi.org/10.1038/nbt.3353 (2015).

20. Utzschneider, K. M., Kratz, M., Damman, C. J. & Hullar, M. Mechanisms Linking the Gut Microbiome and Glucose Metabolism. *J Clin Endocrinol Metab.***101**, 1445–1454 https://doi.org/10.1210/jc.2015-4251 (2016).

21. Bianchi, F., Duque, A. L. R. F., Saad, S. M. I. & Sivieri, K. Gut microbiome approaches to treat obesity in humans. *Appl Microbiol Biotechnol.***103**, 1081–1094 https://doi.org/10.1007/s00253-018-9570-8 (2019).

22. Mortensen, P. B. & Clausen, M. R. Short-chain fatty acids in the human colon: relation to gastrointestinal health and disease. *Scand J Gastroenterol Suppl.***216**, 132–148 https://doi.org/10.3109/00365529609094568 (1996).

23. Gursoy, U. K., Könönen, E. & Uitto, V. J. Prevotella intermedia ATCC 25611 targets host cell lamellipodia in epithelial cell adhesion and invasion. *Oral Microbiol Immunol.***24**, 304–309 https://doi.org/10.1111/j.1399-302X.2009.00510.x (2009).

24. Rams, T. E., Sautter, J. D., Hsiao, C. Y. & van Winkelhoff, A. J. Phenotypic identification of periodontal Prevotella intermedia/nigrescens group isolates validated by MALDI-TOF mass spectrometry. *Anaerobe.***54**, 201–204 https://doi.org/10.1016/j.anaerobe.2018.06.007

(2018).

25. Adeva-Andany, M. M., González-Lucán, M., Donapetry-García, C. & Fernández-Fernández, C. & Ameneiros-Rodríguez, E. Glycogen metabolism in humans. *BBA Clin.***5**, 85–100 https://doi.org/10.1016/j.bbacli.2016.02.001 (2016).

26. Petersen, M. C., Vatner, D. F. & Shulman, G. I. Regulation of hepatic glucose metabolism in health and disease. *Nat Rev Endocrinol.***13**, 572–587 https://doi.org/10.1038/nrendo.2017.80 (2017).

27. Puigserver, P. *et al.* Insulin-regulated hepatic gluconeogenesis through FOXO1-PGC-1alpha interaction. *Nature.***423**, 550–555 https://doi.org/10.1038/nature01667 (2003).

28. Samuel, V. T. *et al.* Fasting hyperglycemia is not associated with increased expression of PEPCK or G6Pc in patients with Type 2 Diabetes. *Proc Natl Acad Sci U S A.***106**, 12121–12126 https://doi.org/10.1073/pnas.0812547106 (2009).

29. Krssak, M. *et al.* Alterations in postprandial hepatic glycogen metabolism in type 2 diabetes. *Diabetes.***53**, 3048–3056 https://doi.org/10.2337/diabetes.53.12.3048 (2004).

30. Kim, Y. J. & Jung, U. J. Honokiol Improves Insulin Resistance, Hepatic Steatosis, and Inflammation in Type 2 Diabetic. *Int J Mol Sci.***20**, https://doi.org/10.3390/ijms20092303 (2019).

31. Wada, T. *et al.* Cilostazol ameliorates systemic insulin resistance in diabetic db/db mice by suppressing chronic inflammation in adipose tissue via modulation of both adipocyte and macrophage functions. *Eur J Pharmacol.***707**, 120–129 https://doi.org/10.1016/j.ejphar.2013.03.016 (2013).

32. Baker, P. J., Dixon, M. & Roopenian, D. C. Genetic control of susceptibility to Porphyromonas gingivalis-induced alveolar bone loss in mice. *Infect Immun.***68**, 5864–5868 https://doi.org/10.1128/iai.68.10.5864-5868.2000 (2000).

33. BLIGH, E. G. & DYER, W. J. A rapid method of total lipid extraction and purification. *Can J Biochem Physiol.***37**, 911–917 https://doi.org/10.1139/o59-099 (1959).

34. Kato, H., Izumi, Y., Hasunuma, T., Matsuda, F. & Kondo, A. Widely targeted metabolic profiling analysis of yeast central metabolites. *J Biosci Bioeng.***113**, 665–673 https://doi.org/10.1016/j.jbiosc.2011.12.013 (2012).

35. Izumi, Y. *et al.* Inter-Laboratory Comparison of Metabolite Measurements for Metabolomics Data Integration. *Metabolites.***9**, https://doi.org/10.3390/metabo9110257 (2019).

36. Ogawa, T., Izumi, Y., Kusumoto, K., Fukusaki, E. & Bamba, T. Wide target analysis of acylglycerols in miso (Japanese fermented soybean paste) by supercritical fluid chromatography coupled with triple quadrupole mass spectrometry and the analysis of the correlation between taste and both acylglycerols and free fatty acids. *Rapid Commun Mass Spectrom.***31**, 928–936 https://doi.org/10.1002/rcm.7862 (2017).

37. Takeda, H. *et al.* Widely-targeted quantitative lipidomics method by supercritical fluid chromatography triple quadrupole mass spectrometry. *J Lipid Res.***59**, 1283–1293 https://doi.org/10.1194/jlr.D083014 (2018).

38. Izumi, Y., Aikawa, S., Matsuda, F., Hasunuma, T. & Kondo, A. Aqueous size-exclusion chromatographic method for the quantification of cyanobacterial native glycogen. *J Chromatogr B Analyt Technol Biomed Life Sci.***930**, 90–97 https://doi.org/10.1016/j.jchromb.2013.04.037 (2013).

39. Sugiyama, N. *et al.* Comparative proteomics of Helicobacter pylori strains reveals geographical features rather than genomic variations. *Genes Cells.***24**, 139–150 https://doi.org/10.1111/gtc.12662 (2019).

40. Rappsilber, J., Mann, M. & Ishihama, Y. Protocol for micro-purification, enrichment, pre-fractionation and storage of peptides for proteomics using StageTips. *Nat Protoc.***2**, 1896–1906 https://doi.org/10.1038/nprot.2007.261 (2007).

41. Werner, T. *et al.* Ion coalescence of neutron encoded TMT 10-plex reporter ions. *Anal Chem.***86**, 3594–3601 https://doi.org/10.1021/ac500140s (2014).

42. Boersema, P. J., Raijmakers, R., Lemeer, S., Mohammed, S. & Heck, A. J. Multiplex peptide stable isotope dimethyl labeling for quantitative proteomics. *Nat Protoc.***4**, 484–494 doi:nprot.2009.21 [pii] https://doi.org/10.1038/nprot.2009.21 (2009).

Declarations

Data availability

Author contributions

YK, SA, and NS are co-first authors and contributed equally to this work. YK devised the study. YK, SA, YS, YN, Yoshihiro Izumi, and NS designed the study protocol. YK, YN, ST, and SH performed mouse and bacterial growth experiments. YS, HU, RY, NS, and Yasushi Ishihama performed proteomic experiments. SA, MT, Yoshihiro Izumi, and TB performed metabolomic experiments. RY, SA, UH, NS and Yasushi Ishihama led the data integration for the bioinformatics analyses and interpreted the analytical outcomes in close collaboration with YK, YN, Yasushi Ishihama, TB, TN, SY, AK, and SM. YK, SA, NS, and Yoshihiro Izumi wrote the manuscript. Yasushi Ishihama, TB, AK, and SM revised the paper. All authors approved the final version of the manuscript. SM is responsible for the integrity of all data.

Tables

Table 1. Food intake and body weight in *Porphyromonas gingivalis* (*Pg*)- and carboxymethyl cellulose control-treated *db/db* mice fed ad libitum, at baseline and 1–4 weeks after treatment.

	Group	Baseline	1 week	2 weeks	3 weeks	4 weeks
Food intake/cage (g)	Control	205 ± 3	208 ± 11	217 ± 4	220 ± 26	204 ± 9
N = 4	*Pg*	205 ± 4	211 ± 10	199 ± 38	208 ± 33	202 ± 38
Body weight (g)	Control	35.3 ± 2.8	38.0 ± 2.0	40.3 ± 2.7	42.4 ± 1.6	43.9 ± 1.8
N = 8	*Pg*	35.0 ± 2.7	37.7 ± 2.5	40.1 ± 2.5	41.5 ± 2.2	43.0 ± 2.7

Data are expressed as means ± standard error of mean. * *P* < 0.05 compared with the control; n = 8.

Table 2. Blood glucose and blood insulin levels under fasting, and serum triglyceride levels under ad libitum feeding, in *Porphyromonas gingivalis* (*Pg*)- and carboxymethyl cellulose control-treated *db/db* mice.

	Blood glucose (mg/dL: fasting)	IRI (µU/mL: fasting)	Triglyceride (mg/dL: ad libitum feeding)
Control	346 ± 124	32.5 ± 18.7	290± 101
Pg	467 ± 124*	36.5 ± 18.7	252± 90

Glucose and insulin levels were measured 3 weeks after treatment, and triglyceride levels 4 weeks after treatment. Data are expressed as means ± standard error of mean. * *P* < 0.05 compared with the control; n = 8. IRI: immunoreactive insulin.

Table 3. Proteome profiling of feces of *Porphyromonas gingivalis* (*Pg*)- and carboxymethyl cellulose control-treated *db/db* mice, giving the numbers of peptides detected.

Category	1st administration		10th administration	
	Pg	Control	*Pg*	Control
All	7,000	6,641	9,064	8,619
Mouse	844	821	1,408	1,276
Bacteria	5,467	5,061	6,601	6,324
Food	689	759	1,019	1,019

For the orally **administrat**ed mice, there was no statistical difference in the number of detected peptides between the *Pg*- and CMC control-treated groups.

Table 4. Distinct peptides derived from *Porphyromonas gingivalis* (*Pg*), identified using proteome analysis of feces of *Pg*-treated *db/db* mice.

Peptide sequence	Corresponding protein
DVTVEGSNEFAPVQNLTGSAVGQK	Hemagglutinin A
ECVNVTVDPVQFNPVQNLTGSAVGQK	Hemagglutinin A
NDSNTSDYSIIFNTLQK	DNA-directed RNA polymerase subunit beta
LQFTGFDIYGFPQGSK	Outer membrane protein 40
VAEDIASPVTANAIQQFVK	Gingipain R1
VLVDNYPLIDVTTAK	Receptor antigen B

Table 5. Intestinal metabolites showing significantly different expression between *Porphyromonas gingivalis* (*Pg*)- and carboxymethyl cellulose control-treated *db/db* mice.

Downregulation

	Control	Pg	Pg / Control	P value
Tyrosine	1897.5 ± 188.1	202.8 ± 125.7	0.11	0.00020
Isoleucine	9.8 ± 0.5	4.1 ± 0.8	0.42	0.00037
Thymidine	3.1 ± 0.5	0 ± 0.0	0.00	0.00052
Spermine	41.8 ± 5.8	4.1 ± 4.4	0.01	0.00087
N-Acetyl glutamine	3.9 ± 0.4	0.9 ± 0.5	0.24	0.00138
Lysine	476.3 ± 95.4	50 ± 26.5	0.10	0.0017
Tryptophan	272 ± 54.5	25.4 ± 19.9	0.09	0.0018
Octopamine	21.3 ± 2.1	6.8 ± 2.8	0.32	0.0021
Arginine	5.3 ± 0.8	0.9 ± 0.8	0.16	0.0021
Arabitol	3.5 ± 0.5	0.9 ± 0.4	0.27	0.0028
Phenylalanine	582.7 ± 105.9	128.7 ± 62.5	0.22	0.0031
Cytosine	10.8 ± 2.8	0.6 ± 0.2	0.06	0.0031
Pantothenic acid	1.5 ± 0.1	0.6 ± 0.2	0.42	0.0033
Arabinose-meto	2.9 ± 0.5	1.2 ± 0.2	0.43	0.0041
Tyramine	4.6 ± 1.3	0.3 ± 0.4	0.05	0.0052
Gluconic acid	29.8 ± 7.0	7.5 ± 1.7	0.25	0.0058
Ornithine	9.9 ± 2.7	1.3 ± 0.4	0.14	0.0056
Dihydroxyacetone	4.5 ± 1.2	1.2 ± 0.0	0.28	0.0089
Leucine	3698.9 ± 971.6	1195 ± 364.4	0.32	0.014
Galacturonic acid	5.6 ± 1.7	1.4 ± 0.4	0.26	0.014
Isoleucine	1246.1 ± 311.5	457 ± 134.2	0.37	0.016
Allantoin	5.3 ± 1.5	1.5 ± 0.8	0.29	0.019
Methionine	44.7 ± 11.8	15.9 ± 5.9	0.36	0.020
Cysteine	133.5 ± 25.5	77.5 ± 6.0	0.58	0.021
Histidine	56 ± 23.8	4.8 ± 3.8	0.09	0.021
Lactose-meto	42.5 ± 16.2	7.4 ± 3.6	0.17	0.022
5-Oxoproline	972.8 ± 136.1	553.9 ± 144.6	0.57	0.022
Ornithine	37.1 ± 6.1	18.5 ± 6.6	0.50	0.023
Pyruvic acid	1.9 ± 0.7	0.6 ± 0.2	0.30	0.028
Asparagine	18.7 ± 7.6	3.4 ± 2.1	0.18	0.029
Valine	1531.3 ± 402.1	723.5 ± 178.2	0.47	0.033
Fructose-meto	28.9 ±	13.7	0.47	0.039

Up

	Control	Pg	Pg / Control	P value
O-Phosphoethanolamine	13.3 ± 2.0	24.9 ± 3.8	1.873601148	0.00931
Lactic acid	965.4 ± 75.9	1449.8 ± 172.4	1.501812664	0.01121
Fructose 1-phosphate	10.8 ± 3.3	29.6 ± 7.0	2.743926554	0.01357
Fructose 1-phosphate	13.2 ± 3.3	28.3 ± 5.4	2.145544825	0.01465
3-Hydroxyisobutyric acid	3.3 ± 1.6	7.6 ± 1.4	2.284343887	0.02438
Phosphoric acid	802.7 ± 151.5	1295 ± 222.7	1.613203304	0.03399
3-Hydroxybutyric acid	9.9 ± 4.9	22.6 ± 5.1	2.297638051	0.03464

	8.5 ± 2.1			
Fructose	46.6 ± 13.6	22.6 ± 2.7	0.49	0.040
Lactose	11.6 ± 5.5	2.1 ± 0.8	0.18	0.042
Glutamic acid	558.7 ± 148.6	243.7 ± 112.5	0.44	0.043
Glutamine	9.8 ± 2.9	3.9 ± 2.2	0.40	0.049

Upregulation

	Control	Pg	Pg / Control	P value
O-Phosphoethanolamine	13.3 ± 2.0	24.9 ± 3.8	1.87	0.010
Lactic acid	965.4 ± 75.9	1449.8 ± 172.4	1.50	0.011
Fructose 1-phosphate	10.8 ± 3.3	29.6 ± 7.0	2.74	0.014
Fructose 1-phosphate	13.2 ± 3.3	28.3 ± 5.4	2.15	0.015
3-Hydroxyisobutyric acid	3.3 ± 1.6	7.6 ± 1.4	2.28	0.024
Phosphoric acid	802.7 ± 151.5	1295 ± 222.7	1.61	0.034
3-Hydroxybutyric acid	9.9 ± 4.9	22.6 ± 5.1	2.30	0.035

Intestinal metabolite levels were measured using metabolome analysis of mixed intestinal tissue and fecal material specimens. Data are expressed as means ± standard error of mean; n = 3.

Figures

Fig. 1a
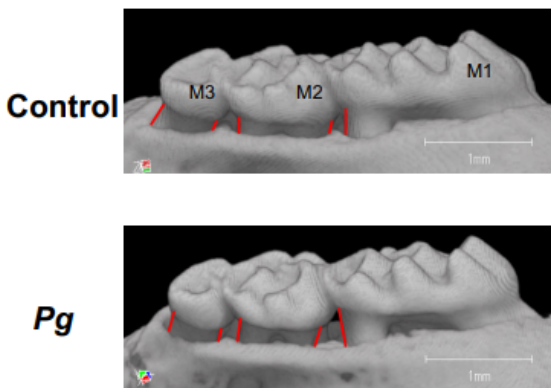
Fig. 1b
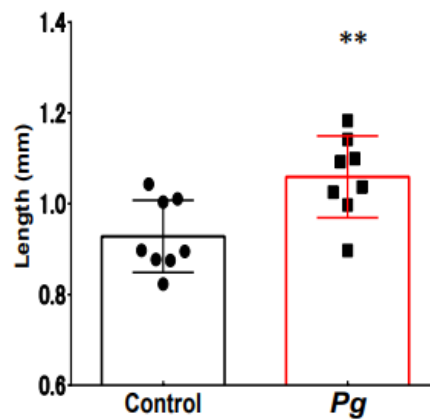
Figure 1

Effects of oral Porphyromonas gingivalis (Pg)-administration on alveolar bone loss in db/db mice (a). Buccal-side maxillary alveolar bone loss (ABL, colored lines), measured from the cementoenamel junction (CEJ) to alveolar bone crest (ABC) at five points: (1) distobuccal regions for first maxillary molar (M1); (2) mesiobuccal and (3) distobuccal regions for second maxillary molar (M2); and (4) mesiobuccal

and (5) distobuccal regions for third maxillary molar (M3), in db/db mice treated with Pg or CMC control for 30 d. (b) Comparison of the sum of the five CEJ-ABC linear distances. ** P < 0.01; n = 8. Data are shown as means ± SEM.
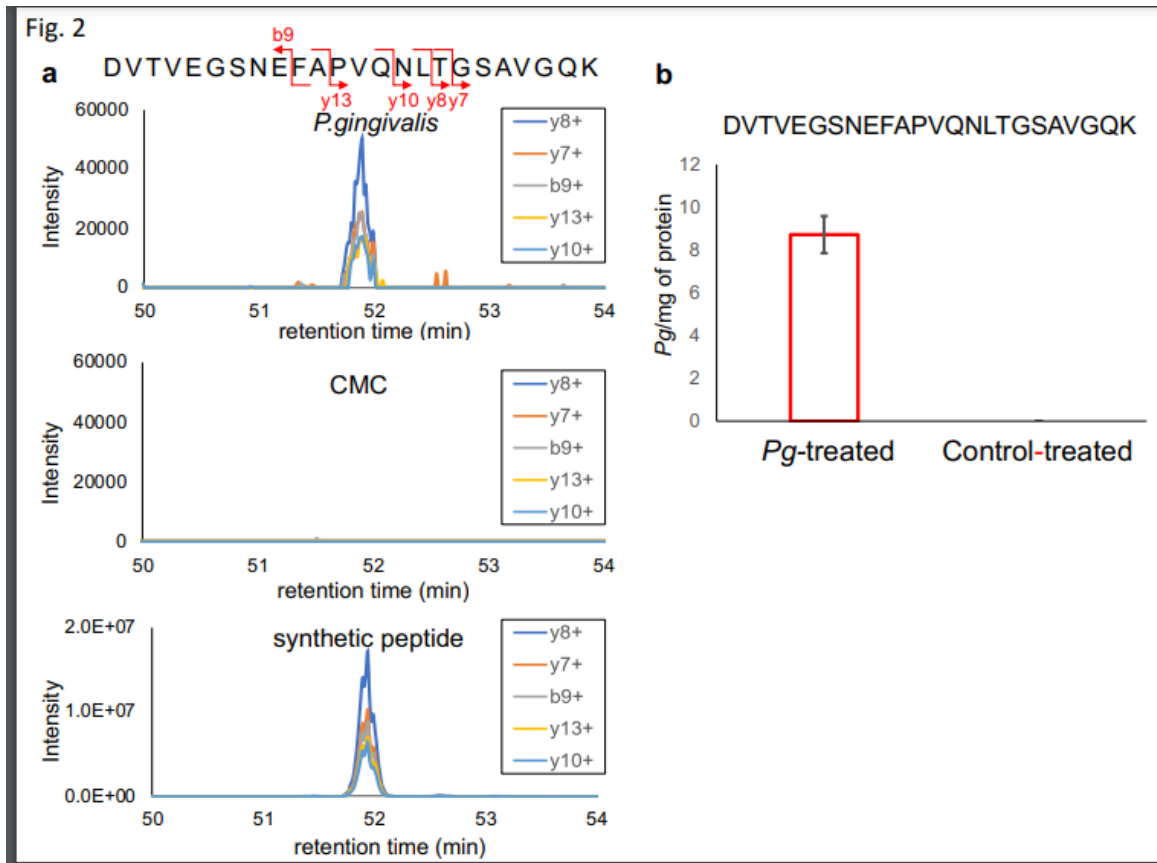
Figure 2

Parallel reaction monitoring analysis of the distinct peptides derived from Porphyromonas gingivalis (Pg). (a) Chromatogram of the fragment ions for the Pg-unique peptide DVTVEGSNEFAPVQNLTGSAVGQK and its five different amino-acid fragments in Pg- or control-treated mouse feces, and of the synthetic peptide used as the internal standard. (b) Detection of this peptide in Pg-treated, but not CMC control-treated, mice, using a synthetic peptide as internal standard. Sample preparation was performed in triplicate from the pooled feces; peptides were quantified based on the median peak area ratio of each fragment ion. (c) Phylum-, (d) family-, and (e) genus-level distributions of the fecal microbiome. Taxonomic assignments of the peptides identified via metaproteome analysis of fecal samples were performed using Unipept. The distributions were profiled based on the number of taxa-specific peptides. 'Control 1 day': CMC control-treated, 1 d after the first injection; 'Control 30 days': CMC control-treated, 30 d after the tenth injection; 'Pg 1 day': Pg-treated, 1 d after the first injection: 'Pg 30 days': Pg-treated, 30 d after the tenth injection.

Fig. 3 Volcano plots of intestinal metabolites in fecal specimens of diabetic mice orally treated with *Pg* compared with those for CMC-treated mice.

Hydrophilic metabolites

$-\log_{10} p\text{-value}$

$\log_2$ Fold change (*Pg*/Control)
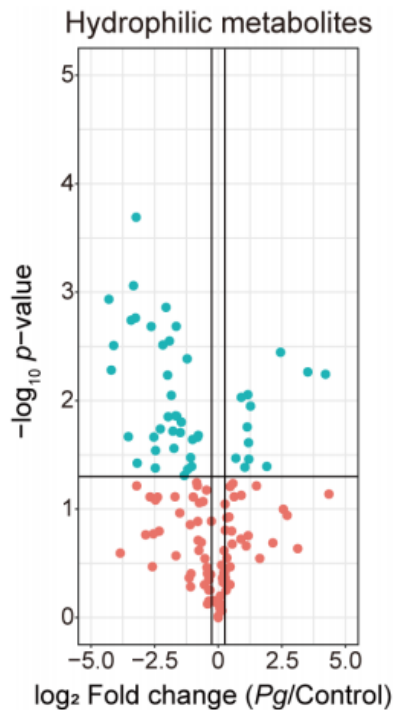
Figure 3

Volcano plot of fold change in intestinal hydrophilic metabolites in fecal specimens of diabetic mice orally treated with Porphyromonas gingivalis (Pg) or CMC (control). Blue points represent a significant increase or decrease.
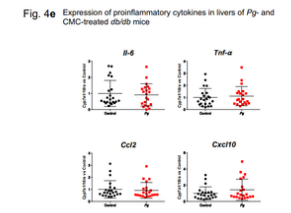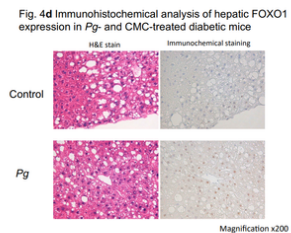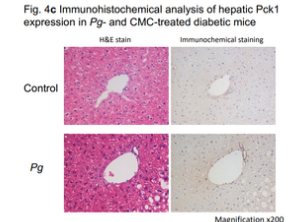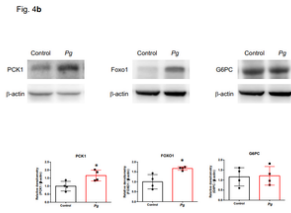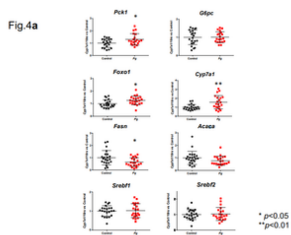
Figure 4

Effects of oral Porphyromonas gingivalis (Pg) administration on mRNA and protein expression in the liver of db/db mice. (a) mRNA expression of Pck1, G6pc, Foxo1, Cyp7a1, Fasn, Acaca, Cpt1, Srebf1, and Srebf2. mRNA expression was determined using quantitative RT-PCR and was normalized against the level of 18S rRNA mRNA. Target gene expression in Pg-treated mice was normalized against the target gene expression in CMC-treated mice, which is considered as 1. Treatment or control group variability was calculated as the ratio of [each amount/the mean amount in the control] in every chart. n = 20−21, ** P < 0.01, * P < 0.05 vs control. (b) Western blot analysis of PCK1, G6PC, and FOXO1 in liver tissues from db/db mice treated with Pg or CMC for 30 days. β-actin was used as the loading control. The bar graphs on the right show densitometric quantification of the amounts of PCK1, G6PC, and FOXO1, relative to the control. n = 4; * P < 0.05 vs control. (c, d) PCK1 (c) and FOXO1 (d) detection in liver tissues of Pg- or control-treated mice. Left column: Paraffin-embedded sections stained with hematoxylin and eosin (H&E). Right column: Immunohistochemical detection; Magnification: 200×. (e) Comparison of relative gene expression of proinflammatory cytokines (Il-6, Tnf-α, Ccl2, and Cxcl10) in liver tissue of Pg- and control-treated db/db mice. The data were normalized and analyzed as described for Figure 4a. n = 20−21. Pck1, Phosphoenolpyruvate carboxykinase 1; G6pc, Glucose-6-phosphatase; Foxo1, Forkhead box protein O1; Cpt1c, Carnitine palmitoyltransferase 1c; Fasn, Fatty acid synthase; Acaca, Acetyl-Coenzyme A carboxylase alpha; Srebf1, Sterol regulatory element-binding transcription factor 1; Srebf2, Sterol regulatory element-binding transcription factor 2; Il-6, Interleukin 6; Tnf-α, Tumor necrosis factor-α; Ccl2, Chemokine (C-C motif) ligand 2; Cxcl10, C-X-C motif chemokine ligand 10.

Fig. 5a Volcano plots of hepatic glucose metabolites in diabetic mice orally treated with Pg compared with those for CMC-treated-mice.
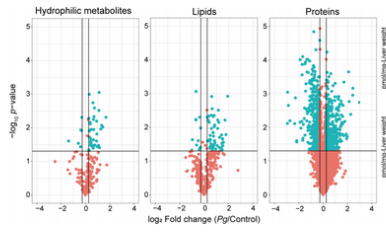
Fig. 5b Changes in hepatic glycogen content and substrate relating to gluconeogenesis in Pg- and CMC-treated diabetic mice
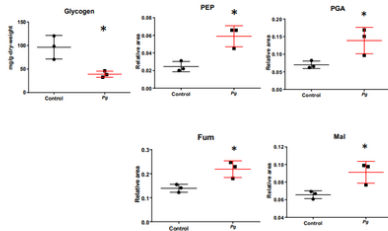
Fig. 5c Hepatic glycogen synthesis and degradation and glycogen content in Pg- and CMC-treated db/db mice
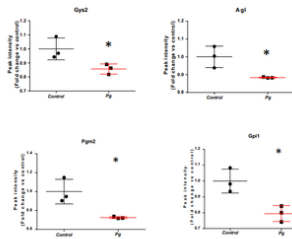
Fig. 5d Changes in hepatic rate-limiting enzymes to regulate gluconeogenesis and glycolysis in Pg- and CMC-treated diabetic mice
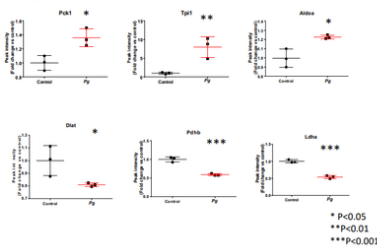
* P<0.05
**P<0.01
***P<0.001

Figure 5

Proteome and metabolome profiles of the livers of db/db mice treated with Porphyromonas gingivalis (Pg) or CMC (control) for 30 days, obtained using nano-LC/MS/MS, in triplicate. (a) Volcano plots of fold change in hydrophilic metabolites, lipids, and proteins, between Pg- and control-treated mice. Blue points represent significant increase or decrease (the relevant compounds are listed in Supplementary Tables S4 and S5−8). (b) Glucose metabolite levels (PEP, PGA, FUM, and MAL) were significantly higher ($P < 0.05$), whereas glycogen content was significantly lower ($P < 0.05$), in Pg-treated than CMC-treated mice. (c) Comparative proteome analysis of glycolysis/gluconeogenesis-related enzyme levels in Pg- and control-treated mice. (d) Comparative proteome analysis of enzyme synthesis and degradation during glycogen and G6P metabolism via the glycolytic pathway, in Pg- and control-treated mice. PCK1, ALDOA, and TPI1 were significantly higher, whereas Pgm2, DLAT, GPI1, LDHA, PDH, Gys2, AGL, and Gpi 1 levels were significantly lower (c, d), in Pg-treated than in control-treated mice. Panels b−d: Data normalized and statistically analyzed as for Fig 4a. n = 3, * $P < 0.05$, ** $P < 0.01$ and *** $P < 0.001$, vs control.
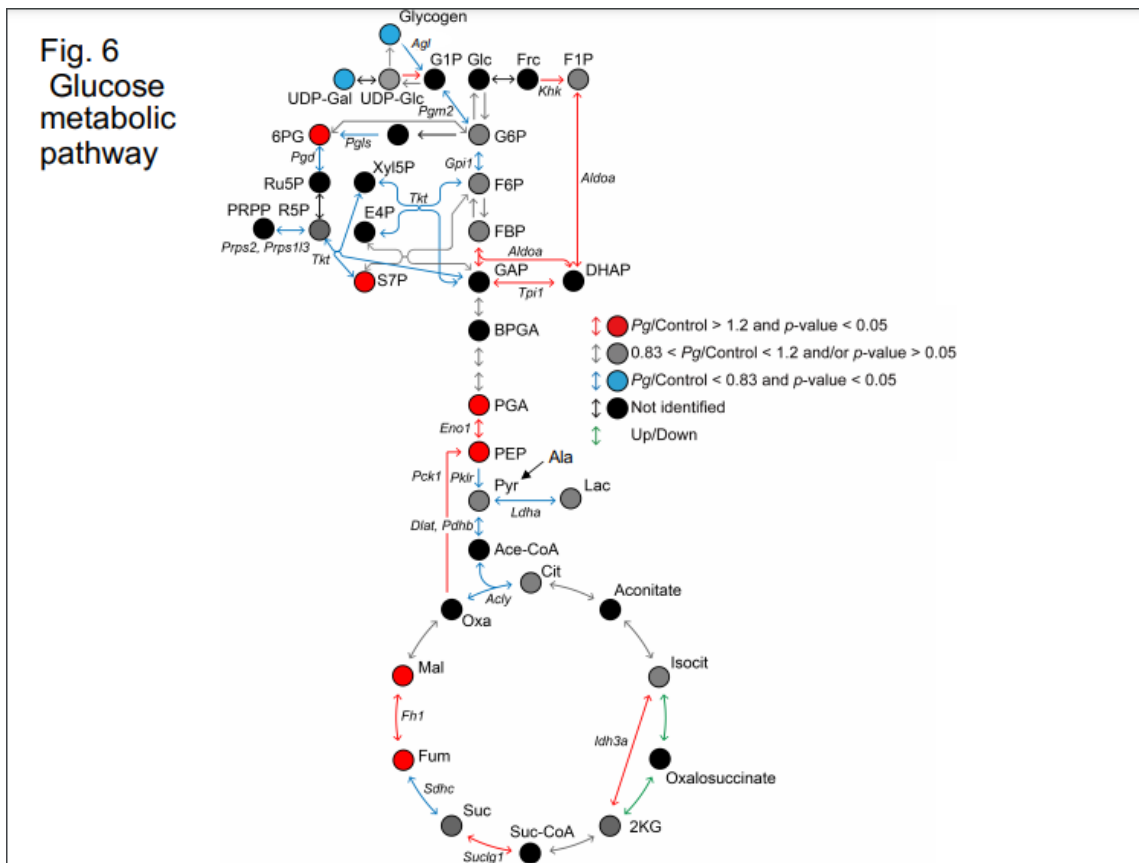
Figure 6

Schematic presentation of hepatic glucose metabolites and the expression of rate-limiting glucose metabolism enzymes in Pg- and CMC-treated diabetic mice. Fold change in the contents of glucose metabolites and enzymes involved in intrahepatic glucose metabolism in Pg-treated mice relative to those in the control. Red circles and lines: significant increases. Blue circles and lines: significant reductions. Metabolites that varied substantially and significantly between the Pg-treated mice and the control were identified using these criteria: log2 fold change > |0.26| and P < 0.05, and P < 0.01. 2KG, 2-Ketoglutaric acid; 6PG, 6-Phosphogluconic acid; Ace CoA, Acetyl-CoA; BPGA, 1,3-Bisphosphoglycerate; Cit, Citric acid; DHAP, Dihydroxyacetone phosphate; F1P, D-Fructose 1-phosphate; F6P, D-Fructose 6-phosphate; Frc, D-Fructose; G1P, D-Glucose 1-phosphate; G6P, D-Glucose 6-phosphate; GAP, Glyceraldehyde 3-phosphate; Glc, D-Glucose; Isocit, Isocitric acid; Lac, Lactic acid; MAL, Malic acid; Oxa, Oxaloacetic acid; PEP, Phosphoenolpyruvic acid; PGA, 2-Phospho-D-glyceric acid/3-Phospho-D-glyceric acid; Pyr, Pyruvic acid; Suc, Succinic acid; Suc CoA, Succinyl-CoA; UDP-Gal, UDP-alpha-D-galactose; UDP-Glc, Uridine 5'-diphosphate glucose; AGL, Amylo-1,6-glucosidase, 4-alpha-glucanotransferase; Aldoa, Fructose-bisphosphate aldolase A; Dlat, Dihydrolipoyllysine-residue acetyltransferase component of pyruvate dehydrogenase complex, mitochondrial; Pdhb, Pyruvate dehydrogenase E1 component subunit beta; Fh1, Fumarate hydratase-1; Gpi1, Glucose-6-phosphate isomerase 1; Gys2: Glycogen [starch] synthase 2; Ldha, L-lactate dehydrogenase; Pck1, Phosphoenolpyruvate carboxykinase; Pgm2, Phosphoglucomutase-2; Idh3a, Isocitrate dehydrogenase [NAD] subunit alpha, mitochondrial; Suclg1, Succinyl-CoA ligase [GDP-forming] subunit alpha, mitochondrial; Sdhc, Succinate dehydrogenase (ubiquinone) cytochrome b560 subunit; Acly, ATP citrate (pro-S)-lyase; Tpi1, Triosephosphate isomerase 1.

Supplementary Files

This is a list of supplementary files associated with this preprint. Click to download.

- SupplementarydatasettableS2fecesproteome.xlsx
- SupplementarydatasettableS4liverproteome.xlsx
- SupplementarydatasettableS5S8livermetabolome.xlsx
- Supplementaryinformation.pdf